ARTICLE

ACS chemical biology

Use of Calculated Cation-π Binding Energies to Predict Relative Strengths of Nicotinic Acetylcholine Receptor Agonists

Mathew Tantama and Stuart Licht*

Department of Chemistry, Massachusetts Institute of Technology, 77 Massachusetts Avenue, Building 16, Room 573B, Cambridge, Massachusetts 02139

ABSTRACT Agonists and antagonists of the nicotinic acetylcholine receptor (nAChR) are used to treat nicotine addiction, neuromuscular disorders, and neurological diseases. In designing small molecule therapeutics with the nAChR as a target, it is useful to identify chemical parameters that correlate with ability to activate the receptor. Previous studies have shown that cation-π interactions at the transmitter binding sites of the nAChR are important for receptor activation by strong agonists such as acetylcholine. We hypothesized that a calculated estimate of cation-π binding ability could be used to predict the efficiency for channel opening (*i.e.*, the gating efficiency) associated with activation of the acetylcholine receptor by a series of structurally related organic cations. We demonstrate that the calculated cation-π energy is strongly correlated with gating efficiency but only weakly correlated with closed-state binding affinity. Our results suggest that cation-π interactions contribute significantly to the open-state affinity of these cations and that the calculated cation-π energy will be a useful parameter for designing nAChR agonists and antagonists.

Nicotinic acetylcholine receptors (nAChRs) are ion channels involved in a broad range of synaptic activities throughout the nervous system and are the targets of therapeutic drugs for a variety of conditions (*1*). These drugs are often agonists or competitive antagonists that bind the nAChR transmitter binding sites (TBSs) in a state-selective manner. A strong agonist exhibits a high affinity for the closed state and an even higher affinity for the open state, promoting the efficient conformational change from the closed state to the open state (*i.e.*, gating). A strong competitive antagonist exhibits a high affinity for the closed state but not for the open state, making gating inefficient. Establishing chemical metrics that correlate with closed-state affinity and open-state affinity may be useful in the design of drugs that modulate nAChR activity. For example, structure−activity relationships (SARs) have been used to develop nAChR antagonists that can be used as muscle relaxants (*2*). However, SAR parameters such as molecular shape, charge, and hydrogen bonding ability have had limited utility in guiding the design of neuromuscular blocking agents. In the brain, nAChRs have been proposed to be targets for treating nicotine addiction, depression, and a variety of neurological disorders (*3*). SARs for these drug candidates are typically centered on derivatives of nAChR agonists or antagonists derived from natural sources, such as nicotine or epibatidine. However, the small molecule drugs that bind nAChRs are structurally very diverse, and the identification of simple, independent parameters that correlate with binding or gating would be useful for expanding the scope of SAR-guided drug design for these targets.

Cation-π binding ability is a computationally accessible parameter that may be useful in this regard. Like

*Corresponding author, lichts@mit.edu.

Received for review August 4, 2008 and accepted September 23, 2008.

Published online November 21, 2008

10.1021/cb800189y CCC: $40.75

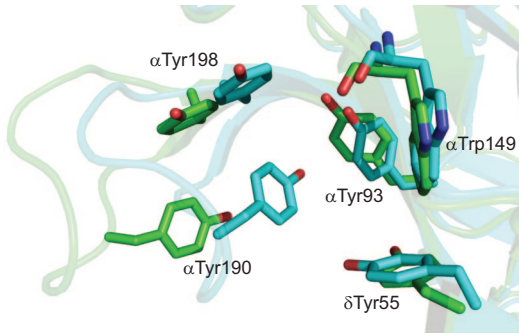

Figure 1. The binding site aromatic cage: green, the apo-AChBP structure (PDB 2BYN); cyan, the epibatidine-bound AChBP structure (PDB 2BYQ). The bound epibatidine molecule has been removed for clarity. In the nAChR itself, δTrp55 takes the place of δTyr55 in the AChBP structure.

hydrogen bonds and salt bridges, cation-π interactions are well-characterized noncovalent interactions that are strong enough (*4–6*) to drive a protein conformational change if that change alters the interaction strength. Cation-π interactions have been shown to be important for the function of nAChRs and other members of the Cys-loop superfamily (*7, 8*). Cation-π interactions between charged small molecules and the nAChR were originally proposed because of the large number of aromatics situated at the TBSs (*9*). The muscle-type nAChR, the archetype for the Cys-loop superfamily, is a pentameric ion channel consisting of two α subunits, a β subunit, a δ subunit, and either a γ or ε subunit. One TBS is situated at the α-δ interface, and a second TBS is situated at the α-γ interface (in fetal receptors) or the α-ε interface (in adult receptors). Structural and biochemical studies of the nAChR and the acetylcholine binding protein (AChBP) have identified an "aromatic cage" at the two TBSs, consisting of residues αTyr93, αTrp149, αTyr190, αTyr198, and δTrp55 (or γ/εTrp55) (*10–17*). When agonist is bound, the aromatic cage is contracted, increasing its favorable contacts with the agonist (Figure 1). Unnatural amino acid mutagenesis has allowed structure–activity studies analogous to those employed in classical physical organic chemistry to be carried out on the nAChR, providing evidence that cation-π interaction is important for binding of agonists (*15–18*). By using unnatural amino acid mutagenesis, αTrp149 was shown to form cation-π interactions with cholinergic agonists (*18, 19*). Substitution of fluorine on the indole ring of this residue increased the concentration necessary for half-maximal nAChR activation, the EC_{50}, for epibatidine and acetylcholine. The observed increase in EC_{50} correlated with the calculated decrease in cation-π binding ability of the fluorinated analogs. A similar correlation was not observed for the other binding site aromatic residues, suggesting that αTrp149 is primarily responsible for the cation-π interaction between acetylcholine and the muscle-type nAChR (*19–21*).

Analogously to K_M in enzyme kinetics, EC_{50} reflects both binding and conformational or chemical equilibria. For an ion channel, the gating equilibrium can be a significant component of EC_{50}. Therefore, the correlation between EC_{50} and cation-π binding energy is consistent with three possibilities. The cation-π energy might contribute entirely to binding/closed-state affinity, indicating that the interaction fully forms when agonist binds the closed state. Alternatively, the cation-π energy might contribute to both binding and gating, indicating that the interaction forms in the closed state and strengthens in the open state. Finally, the cation-π energy might contribute entirely to the open-state affinity (gating), indicating the interaction only exists in the open state. In all three cases, attenuation of the cation-π energy would increase the EC_{50}.

It has been hypothesized that the correlation between EC_{50} and cation-π energy primarily reflects contributions to binding (*18*). Both 5-hydroxytryptamine (5-HT) and acetylcholine (ACh) are strong agonists for the serotonin receptor $5\text{-}HT_{3A}R$, an nAChR-related channel. For both 5-HT and ACh, channel activation is attenuated by fluorination of αTrp149, and EC_{50}'s are linearly correlated with calculated cation-π binding energies for the fluorination series. For all combinations of agonists and mutated receptors, maximal currents of similar magnitude were observed when saturating concentrations of agonist were used, suggesting gating efficiency was not severely compromised (*22*). However, with the strong agonists used in these studies, changes in gating efficiency could lead to relatively small changes in channel maximal currents. The authors of the previous studies therefore did not rule out the possibility that the interaction between agonist and αTrp149 changes with gating (*18, 19, 22*).

To test the hypothesis that cation-π interactions contribute mainly to closed-state binding affinity, we calculated cation-π interaction energies between benzene and a series of organic cations and measured closed-state agonist binding affinity (K_D) and gating efficiency

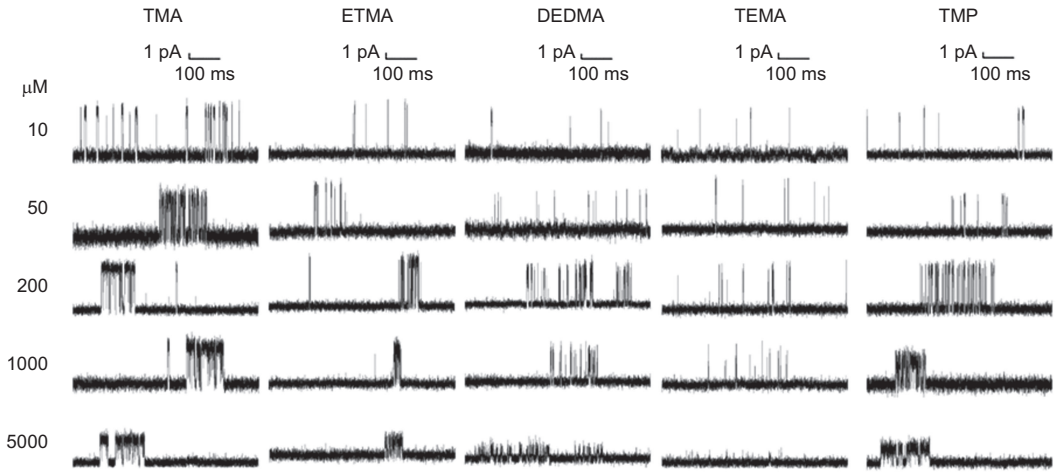

Figure 2. Examples of clustered single-channel activity evoked by the organic cations TMA, ETMA, DEDMA, TEMA, and TMP at concentrations of 10 μM to 5 mM.

(Θ_2) for activation of muscle-type nAChRs by these cations. Single-channel electrophysiology was used to measure microscopic rate constants directly, allowing discrimination of Θ_2 and K_D in the measurements. Small organic cations were used so that the role of the aromatic cage in agonist binding and gating could be probed without having to deconvolve the effect of secondary elements such as the ester moiety of ACh. For the set of compounds tested, there is a strong correlation between the *ab initio* calculated cation-π binding energy and Θ_2, but there is only a weak correlation with K_D. Our results provide evidence that cation-π interactions can be an important factor in determining open state affinity and that calculated cation-π interaction energies have the potential to be used as a parameter in predicting whether small molecules will be nAChR agonists or competitive antagonists.

RESULTS AND DISCUSSION

Activation and Blockade by Organic Cations. To determine binding and gating equilibrium constants for agonists, single-channel activity was first measured as a function of agonist concentration. Single-channel currents from the αG153S nAChR (see Methods) (*23*) were measured using tetramethylammonium (TMA), ethyltrimethylammonium (ETMA), diethyldimethylammonium (DEDMA), triethylmethylammonium (TEMA), and tetramethylphosphonium (TMP) as agonists (Figure 2). Clusters of openings and closings were analyzed to ensure that the kinetics represent the activity of only one chan-

TABLE 1. Dose–Response Parameters

Agonist	P_O^{Max}[a]	EC_{50}[a]	n[a]	K_B[b]	β_2[c]	α_2[d]	K_{Gap}[e]
TMA	0.8 ± 0.03	50 ± 7	1.2 ± 0.1	7000 ± 2000	10300 ± 500	700 ± 70	0.24 ± 0.05
TMP	0.77 ± 0.04	310 ± 50	1.6 ± 0.1	2900 ± 300	5200 ± 100	900 ± 40	0.22 ± 0.08
ETMA	0.6 ± 0.04	80 ± 10	1.7 ± 0.2	2000 ± 100	3400 ± 200	1030 ± 90	0.33 ± 0.09
DEDMA	0.3 ± 0.03	230 ± 60	1.6 ± 0.2	1000 ± 100	380 ± 30	1400 ± 100	1.4 ± 0.4
TEMA[f]	0.03 ± 0.01	400 ± 200	1.5	500 ± 20	60 ± 40	2000 ± 100	30

[a]From a Hill fit of intracluster open probability. EC_{50} in μM. [b]See Figure 3, panel a. K_B in μM. [c]See Figure 3, panel b. β_2 in s^{-1}. [d]See Figure 3, panel c. α_2 in s^{-1}. [e]See Figure 3, panel d. K_{Gap} is unitless. [f]To obtain P_O^{Max}, EC_{50}, and β_2 for TEMA, n was constrained to 1.5. P_O^{Max} was used to calculate K_{Gap} and constrain fitting in Figure 3, panel d to obtain a K_D for TEMA.

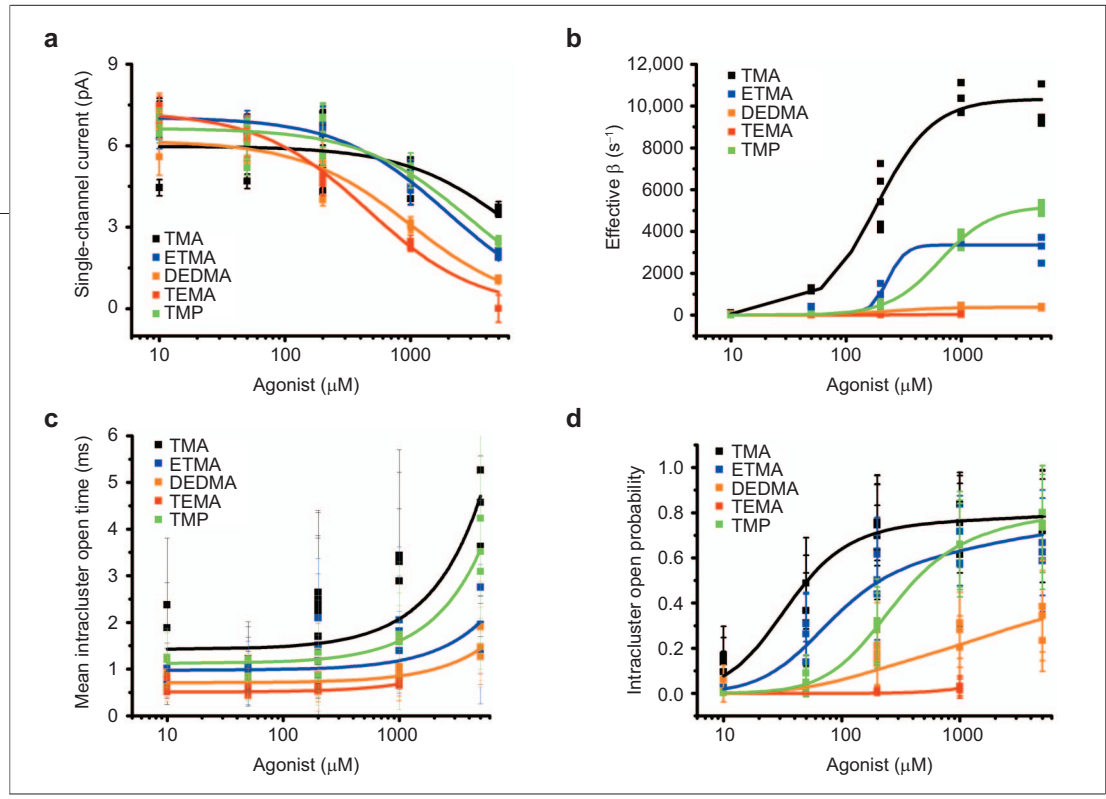

Figure 3. Analysis of single-channel clusters. a) Fast, unresolved open-channel block causes a decrease in apparent single-channel current with increasing agonist concentration. b) The effective opening rate β_2' approaches the true opening rate β_2 as agonist saturates the receptor. c) The closing rate is inversely proportional to the unblocked mean open lifetime. d) Fitting the intracluster open probability using Scheme 1 provides estimates of the closed-state affinity, K_D. TEMA data are also shown with independent scaling in Supporting Information.

nel (*24*). The agonist concentration dependence of the open probability within clusters (P_O) was fitted to a Hill equation (eq 1), where EC_{50} is the concentration for half-maximal open probability and n is the Hill coefficient (Table 1).

$$P_O = P_O^{Max} \cdot \frac{[\text{Agonist}]^n}{EC_{50}^n + [\text{Agonist}]^n} \quad (1)$$

Activation by TEMA was weak, and the Hill coefficient was constrained to a value of 1.5 to produce a reliable fit. Hill coefficients have been generally observed to be 1−2 for nAChR agonists (*25*). In this range, the maximal open probability (P_O^{Max}) varied from 0.028 to 0.053 (see Supporting Information), and the standard deviation of this range of values was used to estimate the uncertainty in P_O^{Max}.

It is important to measure the magnitude of unresolved open-channel blockade because fast blockade will cause an overestimation of open probabilities. Cationic agonists can block the open channel by binding the open pore and interrupting current flow (*26*). When blockade kinetics are sufficiently fast, the current interruptions are unresolved because of limited recording bandwidth, and a reduction in open-channel current at high concentrations is observed (Figure 3). The apparent current amplitude in the presence of unresolved open-channel block is a function of the maximal current in the absence of blocker, i_0, and the blocking dissociation constant, K_B (*27*) (eq 2). The agonist concentration dependence of current amplitude was fitted to obtain K_B (Table 1).

$$i = i_0 \cdot \frac{K_B}{K_B + [\text{Blocker}]} \quad (2)$$

Measurement of Diliganded Gating Rate Constants and Θ_2. The diliganded opening rate constant, β_2, can be measured from the dose−response relationship of the intracluster closed times (Figure 3, Table 1). The ef-

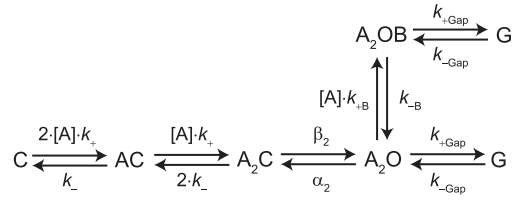

Scheme 1. nAChR model for conformational transitions: C, closed states; O, open states; G, gap states; B, blocked state; A, bound agonist; k_+, association rate constant; k_-, dissociation rate constant; $K_D = k_-/k_+$, dissociation constant; β_2, diliganded opening rate constant; α_2, closing rate constant; Θ_2, gating equilibrium constant; $K_B = k_{-B}/k_{+B}$, blocking dissociation constant; $K_G = k_{+Gap}/k_{-Gap}$, gap equilibrium constant.

TABLE 2. Calculated cation-π energy and measured gating and binding equilibria

Agonist	Cation-π[a]	Θ_2 (s^{-1})	$-R{\cdot}T{\cdot}\ln(\Theta_2)$[b]	K_D[c]	$+R{\cdot}T{\cdot}\ln(K_D)$[d]
TMA	−28.45 ± 0.01	15 ± 2	−6.7 ± 0.3	120 ±20	−22.3 ± 0.4
TMP	−26.97 ± 0.05	5.8 ± 0.3	−4.4 ± 0.1	530 ± 50	−18.7 ± 0.2
ETMA	−27.19 ± 0.19	3.3 ± 0.4	−2.9 ± 0.3	120 ± 10	−22.4 ± 0.3
DEDMA	−26.28 ± 1.80	0.27 ± 0.03	3.3 ± 0.3	110 ± 20	−22.7 ± 0.3
TEMA[d]	−23.31 ± 1.62	0.03 ± 0.02	9 ± 2	200 ± 200	−21 ± 3

[a]Cation-π energies are reported as the mean ± SD for three repeated HF6-31g(d,p)//HF6-31g(d,p) geometry optimizations. [b]Energies in kJ/mol. *R* is the gas constant. *T* = 298.15 K. [c]Dissociation constants in μM. [d]For TEMA, *n* was constrained to 1.5 to obtain an diliganded opening rate constant used to estimate Θ_2, and K_{Gap} was constrained to 30 to obtain and estimate of K_D.

fective opening rate, β_2', reflects gating and agonist binding transitions and is inversely proportional to the major intracluster closed time component, which scales with agonist concentration (*28*). As the agonist concentration increases, the receptor saturates so that β_2' approaches the true opening rate β_2 (eq 3) (*28*). Estimation of β_2 in this manner (*29, 30*) does not require assumption of a specific model.

$$\beta_2' = \beta_2 \cdot \frac{[\text{Agonist}]^n}{K_{\text{Apparent}}^n + [\text{Agonist}]^n} \qquad (3)$$

For TEMA, constraining the Hill coefficient *n* to 1.5 also affects the estimate of β_2. The estimate of β_2 is fairly sensitive to *n*, and the uncertainty in this rate constant was estimated as the standard deviation of values obtained from fits where *n* was constrained to values ranging from 1.0 to 2.0 (see Supporting Information). This procedure gives an estimate of β_2 = 60 ± 40 s^{-1} for activation of the αG153S nAChR by TEMA.

The diliganded closing rate constant α_2 can be estimated from the mean length of single-channel openings. Open lifetimes increased with agonist concentration (Figure 3), consistent with the presence of fast, unresolved open-channel blockade as described above. The increase in mean open lifetime, $<t_O>$, is linearly related to concentration (eq 4). The value of $<t_O>$ in the limit of low blocker concentration represents the unblocked open lifetime and is inversely proportional to the diliganded closing rate constant α_2 (Table 1). Measurement of both the closing and opening rate constants allows determination of the gating equilibrium constant: $\Theta_2 = \beta_2/\alpha_2$ (Table 2).

$$<t_O> = \frac{1}{\alpha_2} + \frac{1}{\alpha_2} \cdot \frac{[\text{Blocker}]}{K_B} \qquad (4)$$

Estimation of K_D From the P_O Dose−Response Curve. The closed state affinities, K_D, were estimated by fitting the P_O dose−response relationships using Scheme 1, with the values of K_B and Θ_2 measured above used as constraints (Figure 3) (*30, 31*). P_O equals the total steady-state occupancy of all open states within the cluster (eq 5) and is a function of the agonist concentration, *A*.

$$P_O = \left[\left(\frac{A^2}{K_D^2}\cdot\Theta_2\right) + \left(\frac{A^2}{K_D^2}\cdot\Theta_2\cdot\frac{A}{K_B}\right)\right] \Big/ \left[1 + \left(\frac{2\cdot A}{K_D}\right) + \left(\frac{A^2}{K_D^2}\right) + \left(\frac{A^2}{K_D^2}\cdot\Theta_2\right) + \left(\frac{A^2}{K_D^2}\cdot\Theta_2\cdot\frac{A}{K_B}\right) + \left(\frac{A^2}{K_D^2}\cdot\Theta_2\cdot K_G\right) + \left(\frac{A^2}{K_D^2}\cdot\Theta_2\cdot\frac{A}{K_B}\cdot K_G\right)\right] \qquad (5)$$

We used the model-independent measurements of K_B and Θ_2 obtained above to constrain the model-dependent analyses, an approach often used to produce physically relevant fitted solutions (*23, 25, 29, 30*). These constraints prevent overparameterization and prevent optimization to values inconsistent with the observed data (Table 2).

Because TEMA is a weak agonist, channel closures were long enough that short-lived desensitization was frequently observed within clusters. An additional constraint was placed on K_G (the equilibrium constant for the short-lived desensitized state) to obtain an estimate of K_D for TEMA. K_G can be set so that the fitted curve saturates at the observed P_O^{Max} (eq 6). From our esti-

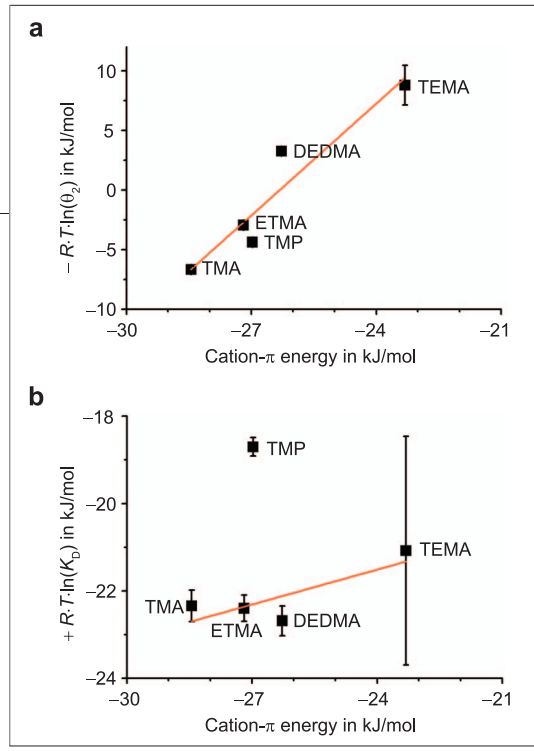

Figure 4. Correlations between calculated cation-π binding energy, gating, and closed-state affinity; red lines represent linear fits. a) Cation-π binding energy is strongly correlated with gating and therefore open-state affinity. b) Cation-π binding energy does not correlate well with closed-state binding affinity.

mate of P_O^{Max} for TEMA, K_G was constrained to a value of 30.

$$P_0^{Max} = \lim P_0 = \frac{1}{1 + K_G} \qquad (6)$$

Because we obtained estimates of P_O^{Max} and Θ_2 for TEMA by constraining the Hill coefficient to $n = 1.5$, we examined the sensitivity of K_D estimation to the values of P_O^{Max} and K_G. Sensitivity analysis of P_O^{Max} and Θ_2 produced a range of 11 values for each parameter (see Supporting Information). We estimated K_D for the 121 possible combinations, and the standard deviation of these 121 values was used to estimate the uncertainty in the dissociation constant for TEMA, $K_D = 200 \pm 200$ μM.

Calculation of Cation-π Interaction Energies. *Ab initio* calculations of benzene−cation complexes were carried out using the Gaussian 03 program (*32*). Geometries were optimized and Hartree−Fock energies were calculated in the gas phase, using the 6-31g(d,p) basis set. The cation-π energies calculated for TMA, ETMA, DEDMA, and TMP were similar, and the calculated energy for TEMA was obviously lower (Table 2). As shown in previous computational studies (*5, 6, 33, 34*), calculated energies for cation-π interactions were comparable to observed gas-phase dissociation energies (*4*). The distance between the cation heteroatom and the benzene ring ranged from 4.8 to 5.0 Å, in agreement with other calculations for quaternary ammoniums (*33, 34*). For all optimized complexes, three α carbons are oriented with protons facing the benzene π system in a facial conformation, as has been previously observed (see Supporting Information) (*33*).

Calculated Cation-π Energy Correlates Strongly with Gating Energy. The calculated cation-π binding energies are linearly correlated with the diliganded gating energies for simple organic cations (Figure 4). Single-channel recording allowed us to experimentally measure the diliganded rate constants α_2 and β_2 for TMA, ETMA, DEDMA, TEMA, and TMP, and the diliganded gating equilibrium, Θ_2, was calculated from these microscopic rate constants. There is a clear linear correlation between cation-π energy and the diliganded gating energy, $-R{\cdot}T{\cdot}\ln(\Theta_2)$. A slope of $m_\Theta = 3.1 \pm 0.6$ ($R^2 = 0.87$) was measured.

Although the slope m_Θ cannot be directly interpreted as a measurement of cation-π interaction energy, it might be expected to be less than unity, since the predicted gas-phase cation-π interaction energy is a reasonable upper limit for the expected interaction energy of a cation solvated by the aqueous/protein environment. The slope $m_\Theta > 1$ suggests that either the calculated cation-π binding energy underestimates the strength of the interaction in the nAChR binding site or multiple cation-π interactions are important to open-state affinity. We used a simple model system to perform *ab initio* calculations of cation-π binding energies between the cations and benzene. In reality, the aromatic cage of the nAChR TBSs contains both tyrosine and tryptophan residues. The cation-π binding ability of benzene and phenol have been calculated to be nearly equal, but an indole has significantly greater cation-π binding potential (*35, 36*). Thus, if the cations are primarily interacting with the indoles of tryptophan residues, our calculations may underestimate the true cation-π binding energy, leading to a slope greater than unity. It is also reasonable to expect that the cation can form cation-π interactions with the multiple aromatic residues when the aromatic cage is compactly arranged in the open state. Although previous studies using unnatural amino acids suggested that the aromatic cage residues other than αTrp149 do not make cation-π interactions with acetylcholine in the muscle-type nAChR (*19, 21*), other studies have shown that different agonists can bind with different favorable contacts (*12, 13,*

18, 22, 37). Notably, residues αTyr190 and αTyr198 appear to be in significantly greater contact with the agonist molecule in bound AChBP structures (*12, 13*). NMR studies also suggest that the cationic head of acetylcholine comes within 3.9 Å of all five aromatic cage residues when bound to the nAChR (*38*).

Calculated Cation-π Energy Correlates Weakly with Close-State Affinity. The calculated cation-π binding energies exhibit only a weak correlation with the closed-state affinity (Figure 4). When the binding energies, $+R{\cdot}T{\cdot}\ln(K_D)$, are plotted versus the calculated cation-π binding energies, TMP is a clear outlier. Even when TMP data are excluded, the correlation is weak (slope $m_K = 0.3 \pm 0.1$, $R^2 = 0.50$; see Supporting Information). The slope m_K is significantly smaller than the slope m_Θ, suggesting that gating is more sensitive than binding to differences in the abilities of simple agonists to form cation-π interactions. These results suggest that the cation-π binding interactions make a relatively small contribution to the total closed-state binding affinity of simple organic cations to the nAChR. However, they do not rule out a role for cation-π interactions in the closed state. The lack of a strong correlation may be due to other factors, such as hydrophobicity (see Supporting Information), having a stronger influence on affinity than the cation-π interaction does.

Implications for the nAChR Binding and Activation Mechanism. The strong linear correlation between calculated cation-π energy and gating energy suggests that cation-π interactions are important for open-state affinity of organic cations to the nAChR TBSs. There is a weak linear correlation between closed-state binding affinities and calculated cation-π energies with a near-zero slope, suggesting other agonist-channel interactions are more important than cation-π interactions in the closed state. Simple organic cations are not positioned for a strong closed-state cation-π interaction by any mechanisms other than partitioning to the binding site and conformational sampling. In contrast, agonist-bound AChBP structures suggest the TBS aromatic cage can assume a compact arrangement around an organic cation in the open state (*12, 13*). The increase in favorable contacts between the cation and aromatics improve positioning for cation-π interactions in the open state.

This mode of binding may differ with other agonists, and the different contributions cation-π energies make to closed-state or open-state affinities for different agonist can be tested. For example, 5-HT and ACh are both more complex than the organic cations investigated here, and cation-π interactions for these strong agonists are hypothesized to contribute primarily to binding rather than channel gating (*18*). For more complex agonists, the structural components separate from the cationic center may help position the molecule for a cation-π interaction in the closed state. For example, the backbone carbonyl of αTrp149 affects activation, an effect that may be due to hydrogen-bonding interactions between the agonist and the carbonyl group (*18*). For 5-HT and ACh, the noncationic moieties might position the cationic center optimally for a strong cation-π interaction. In that case, the strength of the closed-state interaction would be nearly maximal, and the interaction would not strengthen in the open state to a large extent.

Cation-π Interaction Energy as a Parameter for SARs. These results suggest that the calculated cation-π binding energy between a charged agonist and an aromatic ring will be a useful parameter for SARs that distinguish agonists from antagonists. For simple organic cations, we have shown that the cation-π energy is strongly correlated with gating. Thus, similar small molecules that can bind the closed state well but do not form cation-π interactions are likely to be good candidates for activity as antagonists, whereas those that do form such interactions are more likely to be agonists. Cation-π interactions have been shown to impact the function of a broad array of ion channels, both ligand-gated and voltage-gated, and enzymes (*39*). The results of this work thus suggest that calculated cation-π binding energies may be a useful parameter for predicting agonist versus antagonist activity of a variety of drug candidates.

METHODS

Materials. TMA chloride, TEMA chloride, and TMP bromide were from Aldrich. ETMA iodide was from TCI. DEDMA hydroxide from Fluka was neutralized with hydrochloric acid. Cell culture reagents were from Invitrogen. Plasmids for expression of the adult mouse α, β, δ, and ε subunits were generously provided by Professor Anthony Auerbach at SUNY Buffalo (*40*). The gain-of-function αG153S mutation was engineered using site-directed mutagenesis (Quickchange Kit, Qiagen) and verified by sequencing (MIT Biopolymers Laboratory).

Justification for Use of the αG153S Mutant. The organic cations assayed in this work are weak agonists and cause fast

open-channel block of the wild-type nAChR at high concentrations. The advantage of using the αG153S mutant is that it enables clustered single-channel activity to be recorded and analyzed at lower agonist concentrations, where open-channel block is not as severe and can be compensated for in the analysis. The αG153S mutation primarily increases agonist affinity (*23*) by influencing the allosteric transduction mechanism (*41*). Although this mutation occurs at the binding site, it is not part of the aromatic cage. The αG153S mutation is not likely to directly impair the cation-π interaction between αTrp149 and the agonist, and αTrp149 has been shown to be primarily stabilized by αD89 and a redundant hydrogen-bonding network (*42, 43*). Furthermore, the cation-π interaction has been shown to be robust to variations in TBS sequence and structure, existing in several different Cys-loop receptors (*37*). We therefore use this mutant assuming that its effects are equivalent for the series of agonists used here. As a control to demonstrate that the mutation affects the series of cations equivalently, a rate-equilibrium free energy relationship (REFER) was shown to be linear with a slope of approximately 1, as has been observed previously for energetic changes at the TBSs due to mutation or ligand variation (see Supporting Information) (*44, 45*).

Single-Channel Recordings. Adult mouse, muscle-type receptors containing the αG153S mutation were heterologously expressed in HEK-293 cells as previously described (*30*), and single-channel recording was performed in the cell-attached mode (*46*). The bath solution was Dulbecco's phosphate buffered saline (DPBS) containing (in mM): 137 NaCl, 0.9 $CaCl_2$, 0.5 $MgCl_2$, 2.7 KCl, 1.5 KH_2PO_4, 8.1 Na_2PO_4, pH 7.3. Pipette solutions were DPBS supplemented with agonist. Cell membrane potentials were typically −30 to −40 mV, and a command voltage of −70 mV was used during recording. Single-channel currents were amplified with an Axopatch 200B patch-clamp amplifier (Axon Instruments) and recorded through a low-pass Bessel filter at 10 kHz. Data were digitized at a sampling rate of 20 kHz using a NI 6040 E Data Acquisition Board (National Instruments). Data was recorded using QuB software (www.qub.buffalo.edu) (*47–51*). The baselines of single-channel records were adjusted manually using QuB. A 5 kHz Gaussian digital filter was applied, and records were idealized using either the segmental *k*-means or half amplitude algorithms in QuB (*47*). All records were examined visually in their entirety, and misidealizations were corrected manually.

Analysis of Single-Channel Clusters. Single-channel analysis was carried out on clusters of openings as previously described (see Supporting Information) (*30, 31*). At high agonist concentrations, clusters of openings represent activity from one nAChR. Each cluster is a series of openings flanked by long closed durations in which all channels are desensitized. Clusters are defined as those series of openings for which these flanking closed durations are longer than a critical time (τ_{crit}). The value of τ_{crit} is assigned as the intersection of the predominant closed component of the single-channel closed-time distribution and the succeeding component of longer duration. The predominant component scales with agonist concentration and reflects transitions between nAChR closed and open conformations, including binding and gating steps. The value of τ_{crit} was chosen to minimize the percentage of misclassified events, and the fraction of misclassified events was typically less than 5%. Clusters with multiple-conductance levels (more than one channel) or fewer than five events were excluded.

Analysis of clustered activity at the single-channel level allows measurement of microscopic rate constants and distinction of binding and gating steps. To estimate the diliganded closing rate constant α_2, the diliganded opening rate constant β_2, and the diliganded gating equilibrium constant $\Theta_2 = \beta_2/\alpha_2$, the intracluster closed and open dwell-time distributions were analyzed in QuB. To estimate the closed-state affinity K_D, intracluster open probabilities were analyzed according to the equivalent binding sites model shown in Scheme 1. A gap state is included as previously described (*30*). The gap state encompasses short-lived desensitized states that has a lifetime on the order of 1−10 ms (*30*). The gap state is accessible from both the unblocked and blocked open state. The resting and desensitization gates have been shown to be distinct entities (*52, 53*), and it has also been shown that the desensitization gate can close while the open pore is blocked (*54*).

Fitting was performed in Origin (OriginLab, Northhampton, MA).

Computations. *Ab initio* calculations were carried out using the Gaussian 03 program package (*32*). Gas phase calculations have previously been used for investigating the trends in a cation-π perturbation series (*18, 19, 22, 33, 35, 36*). Geometry optimization and Hartree−Fock energies were calculated in the gas phase using the 6-31g(d,p) basis set. As a simple model system, we examined the binding energy trends between benzene and the cations experimentally investigated in this work (*33–36*). The binding energy was estimated as the difference in energies of benzene and the cation optimized separately versus the energy of the pair optimized in complex. The cation was initially placed 4.5 Å above the benzene ring in at least three different orientations; for example, TMA was placed with one, two, or three methyl groups facing the benzene ring. The conformations of the benzene-cation complexes optimized to approximately the same final conformation in each case, and the mean and standard deviation of the calculated binding energies were used throughout the work. No constraints were placed on the conformation of the benzene ring or the benzene-cation distance. The calculated TMA-benzene interaction energy and conformation agreed with the previously published value using this method and basis set (*33*).

Acknowledgment: We thank S. Difley for help with the Gaussian 03 software. This work was supported by the Beckman Foundation and the MIT Department of Chemistry.

Supporting Information Available: This material is free of charge *via* the Internet.

REFERENCES

1. Changeux, J. P., and Taly, A. (2008) Nicotinic receptors, allosteric proteins and medicine, *Trends Mol. Med. 14*, 93–102.
2. Lee, C. (2003) Conformation, action, and mechanism of action of neuromuscular blocking muscle relaxants, *Pharmacol. Ther. 98*, 143–169.
3. Jensen, A. A., Frolund, B., Liljefors, T., and Krogsgaard-Larsen, P. (2005) Neuronal nicotinic acetylcholine receptors: Structural revelations, target identifications, and therapeutic inspirations, *J. Med. Chem. 48*, 4705–4745.
4. Meot-Ner, M., and Deakyne, C. A. (1985) Unconventional ionic hydrogen-bonds. 1. $CH^{\delta+}\cdots X$. Complexes of quaternary ions with normal-donors and π-donors, *J. Am. Chem. Soc. 107*, 469–474.
5. Deakyne, C. A., and Meot-Ner, M. (1999) Ionic hydrogen bonds in bioenergetics. 4. Interaction energies of acetylcholine with aromatic and polar molecules, *J. Am. Chem. Soc. 121*, 1546–1557.
6. Pullman, A., Berthier, G., and Savinelli, R. (1997) Theoretical study of binding of tetramethylammonium ion with aromatics, *J. Comput. Chem. 18*, 2012–2022.
7. Dougherty, D. A. (2008) Cys-loop neuroreceptors: Structure to the rescue? *Chem. Rev. 108*, 1642–1653.
8. Dougherty, D. A. (2008) Physical organic chemistry on the brain, *J. Org. Chem. 73*, 3667–3673.
9. Dougherty, D. A., and Stauffer, D. A. (1990) Acetylcholine binding by a synthetic receptor: Implications for biological recognition, *Science 250*, 1558–1560.

10. Unwin, N. (2005) Refined structure of the nicotinic acetylcholine receptor at 4 Å resolution, *J. Mol. Biol. 346*, 967–989.
11. Brejc, K., van Dijk, W. J., Klaassen, R. V., Schuurmans, M., van Der Oost, J., Smit, A. B., and Sixma, T. K. (2001) Crystal structure of an ACh-binding protein reveals the ligand-binding domain of nicotinic receptors, *Nature 411*, 269–276.
12. Celie, P. H., van Rossum-Fikkert, S. E., van Dijk, W. J., Brejc, K., Smit, A. B., and Sixma, T. K. (2004) Nicotine and carbamylcholine binding to nicotinic acetylcholine receptors as studied in AChBP crystal structures, *Neuron 41*, 907–914.
13. Hansen, S. B., Sulzenbacher, G., Huxford, T., Marchot, P., Taylor, P., and Bourne, Y. (2005) Structures of *Aplysia* AChBP complexes with nicotinic agonists and antagonists reveal distinctive binding interfaces and conformations, *EMBO J. 24*, 3635–3646.
14. Corringer, P. J., Le Novere, N., and Changeux, J. P. (2000) Nicotinic receptors at the amino acid level, *Annu. Rev. Pharmacol. Toxicol. 40*, 431–458.
15. Karlin, A. (2002) Emerging structure of the nicotinic acetylcholine receptors, *Nat. Rev. Neurosci. 3*, 102–114.
16. Sine, S. M., and Engel, A. G. (2006) Recent advances in Cys-loop receptor structure and function, *Nature 440*, 448–455.
17. Lester, H. A., Dibas, M. I., Dahan, D. S., Leite, J. F., and Dougherty, D. A. (2004) Cys-loop receptors: New twists and turns, *Trends Neurosci. 27*, 329–336.
18. Cashin, A. L., Petersson, E. J., Lester, H. A., and Dougherty, D. A. (2005) Using physical chemistry to differentiate nicotinic from cholinergic agonists at the nicotinic acetylcholine receptor, *J. Am. Chem. Soc. 127*, 350–356.
19. Zhong, W., Gallivan, J. P., Zhang, Y., Li, L., Lester, H. A., and Dougherty, D. A. (1998) From *ab initio* quantum mechanics to molecular neurobiology: A cation-π binding site in the nicotinic receptor, *Proc. Natl. Acad. Sci. U.S.A. 95*, 12088–12093.
20. Kearney, P. C., Nowak, M. W., Zhong, W., Silverman, S. K., Lester, H. A., and Dougherty, D. A. (1996) Dose-response relations for unnatural amino acids at the agonist binding site of the nicotinic acetylcholine receptor: Tests with novel side chains and with several agonists, *Mol. Pharmacol. 50*, 1401–1412.
21. Nowak, M. W., Kearney, P. C., Sampson, J. R., Saks, M. E., Labarca, C. G., Silverman, S. K., Zhong, W., Thorson, J., Abelson, J. N., and Davidson, N., *et al.* (1995) Nicotinic receptor binding site probed with unnatural amino acid incorporation in intact cells, *Science 268*, 439–442.
22. Beene, D. L., Brandt, G. S., Zhong, W., Zacharias, N. M., Lester, H. A., and Dougherty, D. A. (2002) Cation-π interactions in ligand recognition by serotonergic (5-HT3A) and nicotinic acetylcholine receptors: The anomalous binding properties of nicotine, *Biochemistry 41*, 10262–10269.
23. Sine, S. M., Ohno, K., Bouzat, C., Auerbach, A., Milone, M., Pruitt, J. N., and Engel, A. G. (1995) Mutation of the acetylcholine-receptor α-subunit causes a slow-channel myasthenic syndrome by enhancing agonist binding affinity, *Neuron 15*, 229–239.
24. Colquhoun, D., and Hawkes, A. G. (1995) The principles of the stochastic interpretation of ion channel mechanisms, in *Single-Channel Recording* (Sakmann, B., and Neher, E., Eds.) 2nd ed., pp 397–482, Plenum Press, New York.
25. Akk, G., and Auerbach, A. (1999) Activation of muscle nicotinic acetylcholine receptor channels by nicotinic and muscarinic agonists, *Br. J. Pharmacol. 128*, 1467–1476.
26. Carter, A. A., and Oswald, R. E. (1993) Channel blocking properties of a series of nicotinic cholinergic agonists, *Biophys. J. 65*, 840–851.
27. Grosman, C., and Auerbach, A. (2000) Asymmetric and independent contribution of the second transmembrane segment 12′ residues to diliganded gating of acetylcholine receptor channels - A single-channel study with choline as the agonist, *J. Gen. Physiol. 115*, 637–651.
28. Auerbach, A. (1993) A statistical analysis of acetylcholine-receptor activation in *Xenopus* myocytes - Stepwise versus concerted models of gating, *J. Physiol. 461*, 339–378.
29. Akk, G., and Steinbach, J. H. (2005) Galantamine activates muscle-type nicotinic acetylcholine receptors without binding to the acetylcholine-binding site, *J. Neurosci. 25*, 1992–2001.
30. Salamone, F. N., Zhou, M., and Auerbach, A. (1999) A re-examination of adult mouse nicotinic acetylcholine receptor channel activation kinetics, *J. Physiol. 516*, 315–330.
31. Purohit, Y., and Grosman, C. (2006) Estimating binding affinities of the nicotinic receptor for low-efficacy ligands using mixtures of agonists and two-dimensional concentration-response relationships, *J. Gen. Physiol. 127*, 719–735.
32. Frisch, M. J. T., G. W.; Schlegel, H. B.; Scuseria, G. E.; Robb, M. A.; Cheeseman, J. R.; Montgomery, Jr., J. A.; Vreven, T.; Kudin, K. N.; Burant, J. C.; Millam, J. M.; Iyengar, S. S.; Tomasi, J.; Barone, V.; Mennucci, B.; Cossi, M.; Scalmani, G.; Rega, N.; Petersson, G. A.; Nakatsuji, H.; Hada, M.; Ehara, M.; Toyota, K.; Fukuda, R.; Hasegawa, J.; Ishida, M.; Nakajima, T.; Honda, Y.; Kitao, O.; Nakai, H.; Klene, M.; Li, X.; Knox, J. E.; Hratchian, H. P.; Cross, J. B.; Bakken, V.; Adamo, C.; Jaramillo, J.; Gomperts, R.; Stratmann, R. E.; Yazyev, O.; Austin, A. J.; Cammi, R.; Pomelli, C.; Ochterski, J. W.; Ayala, P. Y.; Morokuma, K.; Voth, G. A.; Salvador, P.; Dannenberg, J. J.; Zakrzewski, V. G.; Dapprich, S.; Daniels, A. D.; Strain, M. C.; Farkas, O.; Malick, D. K.; Rabuck, A. D.; Raghavachari, K.; Foresman, J. B.; Ortiz, J. V.; Cui, Q.; Baboul, A. G.; Clifford, S.; Cioslowski, J.; Stefanov, B. B.; Liu, G.; Liashenko, A.; Piskorz, P.; Komaromi, I.; Martin, R. L.; Fox, D. J.; Keith, T.; Al-Laham, M. A.; Peng, C. Y.; Nanayakkara, A.; Challacombe, M.; Gill, P. M. W.; Johnson, B.; Chen, W.; Wong, M. W.; Gonzalez, C.; and Pople, J. A. (2004) *Gaussian 03, Revision B.05*, Gaussian, Inc., Wallingford, CT.
33. Lee, J. Y., Lee, S. J., Choi, H. S., Cho, S. J., Kim, K. S., and Ha, T. K. (1995) *Ab initio* study of the complexation of benzene with ammonium cations, *Chem. Phys. Lett. 232*, 67–71.
34. Gao, J., Chou, L. W., and Auerbach, A. (1993) The nature of cation-π binding interactions between tetramethylammonium ion and benzene in aqueous solution, *Biophys. J. 65*, 43–47.
35. Mecozzi, S., West, A. P., and Dougherty, D. A. (1996) Cation-π interactions in aromatics of biological and medicinal interest: Electrostatic potential surfaces as a useful qualitative guide, *Proc. Natl. Acad. Sci. U.S.A. 93*, 10566–10571.
36. Mecozzi, S., West, A. P., and Dougherty, D. A. (1996) Cation-π interactions in simple aromatics: Electrostatics provide a predictive tool, *J. Am. Chem. Soc. 118*, 2307–2308.
37. Mu, T. W., Lester, H. A., and Dougherty, D. A. (2003) Different binding orientations for the same agonist at homologous receptors: A lock and key or a simple wedge? *J. Am. Chem. Soc. 125*, 6850–6851.
38. Williamson, P. T., Verhoeven, A., Miller, K. W., Meier, B. H., and Watts, A. (2007) The conformation of acetylcholine at its target site in the membrane-embedded nicotinic acetylcholine receptor, *Proc. Natl. Acad. Sci. U.S.A. 104*, 18031–18036.
39. Ma, J. C., and Dougherty, D. A. (1997) The cation-π interaction, *Chem. Rev. 97*, 1303–1324.
40. Sine, S. M. (1993) Molecular dissection of subunit interfaces in the acetylcholine receptor: Identification of residues that determine curare selectivity, *Proc. Natl. Acad. Sci. U.S.A. 90*, 9436–9440.
41. Grutter, T., de Carvalho, L. P., Le Novere, N., Corringer, P. J., Edelstein, S., and Changeux, J. P. (2003) An H-bond between two residues from different loops of the acetylcholine binding site contributes to the activation mechanism of nicotinic receptors, *EMBO J. 22*, 1990–2003.
42. Lee, W. Y., and Sine, S. M. (2004) Invariant aspartic acid in muscle nicotinic receptor contributes selectively to the kinetics of agonist binding, *J. Gen. Physiol. 124*, 555–567.

43. Cashin, A. L., Torrice, M. M., McMenimen, K. A., Lester, H. A., and Dougherty, D. A. (2007) Chemical-scale studies on the role of a conserved aspartate in preorganizing the agonist binding site of the nicotinic acetylcholine receptor, *Biochemistry 46*, 630–639.
44. Grosman, C., Zhou, M., and Auerbach, A. (2000) Mapping the conformational wave of acetylcholine receptor channel gating, *Nature 403*, 773–776.
45. Purohit, P., Mitra, A., and Auerbach, A. (2007) A stepwise mechanism for acetylcholine receptor channel gating, *Nature 446*, 930–933.
46. Hamill, O. P., Marty, A., Neher, E., Sakmann, B., and Sigworth, F. J. (1981) Improved patch-clamp techniques for high-resolution current recording from cells and cell-free membrane patches, *Pflugers Arch. 391*, 85–100.
47. Qin, F. (2004) Restoration of single-channel currents using the segmental k-means method based on hidden Markov modeling, *Biophys. J. 86*, 1488–1501.
48. Qin, F., Auerbach, A., and Sachs, F. (1996) Estimating single-channel kinetic parameters from idealized patch-clamp data containing missed events, *Biophys. J. 70*, 264–280.
49. Qin, F., Auerbach, A., and Sachs, F. (1996) Idealization of single-channel currents using the segmental K-means method, *Biophys. J. 70*, 432–432.
50. Qin, F., Auerbach, A., and Sachs, F. (1997) Maximum likelihood estimation of aggregated Markov processes, *Proc. Biol. Sci. 264*, 375–383.
51. Qin, F., and Li, L. (2004) Model-based fitting of single-channel dwell-time distributions, *Biophys. J. 87*, 1657–1671.
52. Auerbach, A., and Akk, G. (1998) Desensitization of mouse nicotinic acetylcholine receptor channels. A two-gate mechanism, *J. Gen. Physiol. 112*, 181–197.
53. Wilson, G., and Karlin, A. (2001) Acetylcholine receptor channel structure in the resting, open, and desensitized states probed with the substituted-cysteine-accessibility method, *Proc. Natl. Acad. Sci. U.S.A. 98*, 1241–1248.
54. Purohit, Y., and Grosman, C. (2006) Block of muscle nicotinic receptors by choline suggests that the activation and desensitization gates act as distinct molecular entities, *J. Gen. Physiol. 127*, 703–717.